RSC Advances

PAPER

View Article Online
View Journal | View Issue

Cite this: *RSC Adv.*, 2026, **16**, 28743

Single crystal X-ray-structurally characterized Mo(VI) complexes of thiophene-appended amide–imine conjugates for optical recognition of calcon and 2-aminobutyric acid

Sangita Maji, Prasenjit Mandal, Amit Kumar De, Sudeshna Chatterjee and Debasis Das *

Two thiophene-appended amide–imine conjugates, *viz.*, thiophene-2-carboxylic acid (3,5-ditertiarybutyl-2-hydroxybenzylidine)hydrazide (**L1**) and thiophene-2-carboxylic acid (3-ethoxy-2-hydroxybenzylidine) hydrazide (**L2**), have been prepared by the condensation of thiophene-2-carboxylic acid hydrazide (**TCA**) with the respective aldehydes. **L1** and **L2** have further been employed for the synthesis of the corresponding Mo(VI) complexes (**M1** and **M2**, respectively). The structures of **M1** and **M2** have been confirmed by single-crystal X-ray diffraction analysis. Fluorescence spectroscopic studies indicate that **M1** and **M2** efficiently and selectively recognize calcon and 2-aminobutyric acid, respectively. The proposed sensing mechanism involves the displacement of the ligands from **M1** and **M2** by the respective analytes. The displacement binding constants are 6.2×10^3 M^{-1} (for calcon) and 12.9×10^4 M^{-1} (for 2-aminobutyric acid). The detection limits for calcon and 2-aminobutyric acid are 6 nM and 5 nM, respectively, in DMSO/H_2O (4/1, v/v, pH 7.4).

Received 12th March 2026
Accepted 7th May 2026

DOI: 10.1039/d6ra02104b

rsc.li/rsc-advances

Introduction

Amide functionality plays a significant role in medicinal chemistry as the backbone of peptides, being present in ~25% of drug molecules.[1–3] In addition, the conformational diversity of the amide moiety has useful implications in synthetic chemistry.[4–10]

On the other hand, transition metal complexes with variable oxidation states may serve as catalysts for the synthesis of bioactive materials.

The dioxomolybdenum(VI) complexes derived from N,O-donor hydrazide derivatives possess interesting stereochemical and microelectronic features.[11] Research interest in dioxomolybdenum(VI) complexes is mainly due to the presence of the molybdenum ion in several enzymes. Apart from structural and biocatalytic studies, the application of molybdenum(VI) complexes as fluorescence probes, operating *via* the ligand-displacement protocol, remains underexplored.

On the other hand, calcon, a naphthalene-based azo dye, is a widely used coloring agent in the textile, food, paper, leather and pharmaceutical industries.[12–14] It is also used as a metal-ion indicator in the laboratory.[15] Consequently, the disposal of industrial effluents containing this toxic dye is a major threat to the environment, and hence, the treatment of industrial waste to remove the dye is necessary before it is released into the environment.[16–25]

Among several analytical methods for the trace-level detection of analytes, fluorescence is considered one of the most effective and versatile method due to its several advantages, *viz.*, operational simplicity, instantaneous response and perception, low operational cost, high sensitivity and selectivity, non-invasive methodology and low detection limit.[26–32]

There is an urgent need for the development of fluorescence probes for trace-level detection and determination of calcon. The literature indicates that calcon is used as a liquid complexing agent in the determination of MoO_3 (Mo^{VI}) by adsorptive stripping voltammetry.[33] The strong Lewis acidity and oxophilic nature of Mo(VI) allow it to interact effectively with incoming analytes that contain hard O-donors, facilitating the ligand-displacement process, the basis of the fluorescence sensing mechanism in the present work.

Moreover, fluorescence detection of calcon using an Mo(VI) complex as a probe has not been reported, and the selectivity issues towards structurally similar dyes remain insufficiently addressed.

Herein, we have explored a Mo(VI) complex, **M1**, for the recognition of calcon *via* "turn-on fluorescence" without any significant interference from competing prototype dyes/coloring agents. The spectroscopic data indicate that calcon sensing proceeds *via* "ligand displacement", where the amide–

Department of Chemistry, The University of Burdwan, Golapbag, Burdwan, W.B., 713104, India. E-mail: ddas100in@yahoo.com; Fax: +91-342-2530452; Tel: +91-342-2533913 ext. 424

imine conjugate, **L1**, is displaced from **M1** by calcon to result in the corresponding Mo(VI)–calcon complex, leading to fluorescence enhancement.[34,35]

On the other hand, it is well known that several metal complexes have the potential to recognize biomolecules.[36,37] 2-Aminobutyric acid, an optically active, non-proteinogenic α-amino acid, is a chiral reagent whose L-(+) form is used in the biosynthesis of non-ribosomal peptides and acts as a receptor antagonist. Further, it is used in the determination of glutamyl cysteine acid synthase and as a drug intermediate.

Literature indicates that several amino acids bind to transition metals,[38] including Mo(VI).[39] In the present report, a new Mo(VI) complex, **M2**, selectively detects 2-aminobutyric acid *via* fluorescence enhancement, where 2-aminobutyric acid replaces **L2** from **M2**,[40] according to the "ligand-displacement" protocol. No significant interference from common amino acids or biomolecules was observed.

Fluorescence detection and determination of an azo dye, namely, calcon, and a biomolecule, 2-aminobutyric acid, is reported for the first time, according to the ligand-displacement protocol.

This present work also demonstrates that tuning a ligand platform of Mo(VI) complexes drastically changes the selectivity in optical sensing to allow the interference-free determination of the analyte.

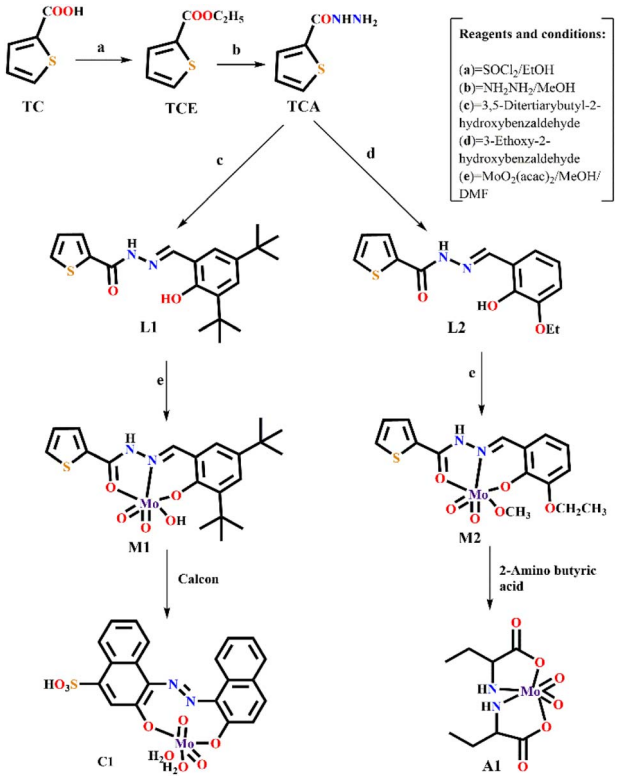

Scheme 1 Synthesis of TCA, M1, M2, C1 and A1.

Experimental

Methods and materials

3-Ethoxysalicylaldehyde, 3,5-ditertiarybutylsalicylaldehyde, metal salts, hydrazine hydrate and PBS buffer were purchased from Sigma Aldrich and Merck. Spectroscopic-grade solvents were used. The mass spectra were recorded using a QTOF 60 Micro YA 263 mass spectrometer in the ES(+) mode. A Shimadzu FTIR (model IR Prestige 21 CE) spectrometer was employed to record FTIR spectra. A Shimadzu UV-2450 spectrophotometer and a quartz cell with a 1 cm path length were used to record absorption spectra. A Hitachi F-7000 spectrofluorometer was used to record fluorescence spectra. A PerkinElmer 2400 Series II CHN analyzer was employed for elemental analysis. The solution pH was measured using a Systronics digital pH meter (model 335). ^{1}HNMR spectra were recorded using a Bruker ADVANCE III HD (400 MHz) spectrometer in DMSO-d_6 solvent. The solvent peak (ppm) was used as an internal reference. The following symbols represent multiplicity: s (singlet), d (doublet), t (triplet), q (quartet), and m (multiplet). Coupling constants (J, s) have been reported in Hertz (Hz).

Single-crystal X-ray diffraction data were collected on a Bruker X8 APEX-II CCD diffractometer at 100(2)K using graphite-monochromated Mo Kα radiation (0.71073 Å). Data were processed and corrected for Lorentz and polarization absorption effects. The crystal structures of **M1** and **M2** were solved by standard direct methods using SHELXS[41] and refined by full-matrix least squares with the SHELXL[42] and OLEX2 (ref. 43) software. Anisotropic thermal displacements were used for the refinement of all non-hydrogen atoms. For structure-factor calculations, the hydrogen atoms were placed in geometrically idealized positions and refined using a riding model, with thermal parameters depending on the parent atom. Images are generated by the Mercury and ORTEP softwares.[44] Significant crystal parameters and refinement data are shown in Table S1 (SI).

Synthesis

Thiophene-2-carboxylic acid hydrazide (TCA). To an ethanolic solution of thiophene-2-carboxylic acid (1 g, 7.03 mmol), a few drops of $SOCl_2$ were added under stirring conditions at room temperature (Scheme 1). The resulting mixture was allowed to react with hydrazine hydrate to produce the corresponding hydrazide (TCA) in 68% yield. Its molecular formula is $C_5H_6N_2OS$ (MW = 142.18). Anal. found (%), C, 42.20, H, 4.18, and N, 19.64; calcd. (%), C, 42.24, H, 4.25, and N, 19.70. ESI-MS(+), m/z $[M]^+$, 142.30, $[M + MeOH + 2H]^+$, 176.4 (Fig. S1a, SI). ^{1}HNMR (Fig. S1b, SI), DMSO-d_6, TMS, δ (ppm): 9.14 (1H, s), 7.17–7.15 (1H, d, $J = 8$), 7.03–7.01 (1H, d, $J = 8$), 6.87–6.83 (1H, t, $J = 8$), 4.08–4.07 (2H, d, $J = 4$). ^{13}CNMR (Fig. S1c, SI): 166.52, 161.39, 147.51, 130.20, and 121.69. FTIR (KBr, cm^{-1}): 3433, ν(N–H); 2919, ν(C–H, aromatic); 1679, ν(C=O); 1117, ν(N–N) (Fig. S1d, SI).

Thiophene-2-carboxylic acid (3,5-ditertiarybutyl-2-hydroxybenzylidine)-hydrazide (L1). A methanol solution containing TCA (142 mg, 1.0 mmol) and 3,5-ditertiarybutyl-2-hydroxybenzaldehyde (172 mg, 1.0 mmol) was refluxed for 6 h. The resulting pale-yellow solution was subjected to slow evaporation, and the pale-yellow solid of **L1** was collected in 78% yield after a few days (Scheme 1). Its molecular formula is $C_{20}H_{26}N_2O_2S$ (MW = 358.17). Anal. found (%), C, 66.20, H, 6.82 and N, 7.11;

calcd. (%), C, 67.01, H, 7.31 and N, 7.81. ESI-MS (*m*/*z*): $[M + H]^+$, 359.16 (Fig. S2a, SI). ^{1}HNMR (DMSO-d_6, 400 MHz): 12.25 (1H, s), 12.11 (1H, s), 8.90 (1H, s), 7.96 (1H, s), 7.87 (1H, s), 7.63–7.62 (2H, d, $J = 4$), 7.51–7.50 (1H, d, $J = 4$), 7.23–7.21 (1H, m, $J = 8$), 1.36 (9H, s). 1.30 (9H, s) (Fig. S2b, SI). ^{13}CNMR (Fig. S2c, SI): 157.97, 148.16, 141.31, 138.14, 135.26–135.04, 132.61, 129.66, 128.70, 127.12, 121.15, 118.03, 115.61, 114.50, 64.61 and 15.20. FTIR (KBr, cm^{-1}): 3234, ν(O–H); 2957, ν(C–H, aromatic); 1626, ν(C=O); 1539, ν(C=N); 1154, ν(N–N) (Fig. S2d, SI).

Thiophene-2-carboxylic acid (3-ethoxy-2-hydroxybenzylidine)-hydrazide (L2). A mixture of thiophene-2-carboxylic acid hydrazide (TCA) (142 mg, 1 mmol) and 3-ethoxy-2-hydroxybenzaldehyde (166 mg, 1 mmol) in methanol was refluxed for 6 h. The resulting solution was allowed to evaporate slowly to produce yellow **L2** in 82% yield. Its molecular formula is $C_{14}H_{14}N_2O_3S$ (MW = 290.07). Anal. found (%), C, 57.42, H, 4.06 and N, 9.12, calcd., C, 57.92, H, 4.86 and N, 9.65. ESI-MS (*m*/*z*): $[M + H]^+$, 291.03, $[M + Na]^+$, 313.01 (Fig. S3a, SI). ^{1}HNMR (DMSO-d_6): 12.11 (1H, s), 11.78 (1H, s), 8.64 (1H, s), 7.97–7.96 (1H, d, $J = 4$), 7.93–7.92 (1H, d, $J = 4$), 7.50–7.48 (1H, d, $J = 8$), 7.26–7.24 (1H, t, $J = 4$), 7.17–7.15 (1H, d, $J = 8$), 7.04–6.99 (1H, t, $J = 8$), 4.09–4.04 (2H, q, $J = 8$), 1.38–1.34 (3H, t, $J = 8$), (Fig. S3b, SI). ^{13}CNMR (Fig. S3c, SI): 162.87, 161.46, 155.11, 150.77, 140.80, 136.06, 131.87, 130.21, 126.01, 123.51, 117.58, 115.64, 52.07 and 31.77. FTIR (KBr, cm^{-1}): 3561, ν(O–H); 3076, ν(C–H, aromatic); 1641, ν(C=O); 1574, ν(C=N); 1144, ν(N–N) (Fig. S3d, SI).

M1 and M2. Methanol solutions of $MoO_2(acac)_2$ (1 g, 3.04 mmol, 5 mL) were added separately to **L1** (0.5 g, 1.39 mmol, 10 mL) and **L2** (0.5 g, 1.72 mmol, 1.39 mmol, 10 mL) in MeOH-DMF (2 : 1, v/v) under stirring conditions for 2 h (Scheme 1). Red crystals of **M1** and **M2** were obtained upon slow evaporation of the solvent.

M1: yield, 62%, molecular formula, $C_{20}H_{24}MoN_2O_5S$ (MW = 533). Anal. found (%), C, 49.02, H, 5.96 and N, 4.86; calcd., C, 49.62, H, 6.06 and N, 5.26. ESI-MS (*m*/*z*): $[M + 3H]^+$, 536.03 (Fig. S4a, SI). FTIR (KBr, cm^{-1}): 2882.49, ν(C–H, aromatic); 1600, ν(C=O); 1445, ν(C=N); 1094, ν(N–N) (Fig. S4b, SI). The structure of **M1** was authenticated by SC-XRD analysis.

M2: yield, 68%, molecular formula, $C_{14}H_{12}MoN_2O_6S$ (MW = 448). Anal. found (%), C, 42.21, H, 4.05 and N, 4.96. calcd., C, 42.68; H, 4.64 and N, 5.86. ESI-MS (*m*/*z*): $[M]^+$, 448.12 (Fig. S5a, SI), $[M + 2H]^+$, 450.12. FTIR (KBr, cm^{-1}): 2947, ν(C–H, aromatic); 1602, ν(C=O); 1506, ν(C=N); 1107, ν(N–N) (Fig. S5b, SI). The structure of **M2** was authenticated by SC-XRD analysis.

C1 (M1-calcon adduct) and A1 (M2-2-aminobutyric acid adduct). To two separate systems of magnetically stirred DMSO/H_2O (1 : 1, v/v) solutions of **M1** and **M2**, a DMSO solution of calcon and an aqueous solution of 2-aminobutyric acid were added dropwise for 5 minutes. The mixtures were kept undisturbed to facilitate slow evaporation and yielded **C1** and **A1**, respectively, the details of which are presented below.

C1: molecular formula, $C_{20}H_{16}N_2O_9SMo$ (MW = 556). ESI-MS (*m*/*z*): $[M + H_2O]^+$, 574.83; $[L1 + Li + 2H]^+$, 366.94 for displaced **L1** (Fig. S6a, SI). FTIR (KBr, cm^{-1}): 3235, ν(O–H); 2963, ν(C–H, aromatic); 1631, ν(C=C); 1434, ν(N=N), 1284, ν(C–N) (Fig. S6b, SI).

A1: molecular formula, $C_8H_{16}N_2O_6Mo$ (MW = 332.16). ESI-MS (*m*/*z*): $[M + 3H]^+$, 333.92; $[L2]^+$ 290.99 for displaced **L2** (Fig. S7a, SI). FTIR (KBr, cm^{-1}): 3430, ν(N–H); 1608, ν(C=O); 1256, ν(C–N) (Fig. S7b, SI).

Results and discussion

X-ray diffraction analysis

The ORTEP views of **M1** (CCDC 2365489) and **M2** (CCDC 2365810) are presented in Fig. 1. Both **M1** and **M2** possess distorted octahedral geometry. A summary of the crystallographic refinement parameters is presented in Table S1 (SI). Important bond lengths and angles are provided in Table S2a and b (SI).

In **M1**, bond lengths of amide C–O, O005–C00H (1.310(7)Å) and phenol C–O, O004–C00B (1.343(7)Å) are very close and indicate the C–O single bond character. Thus, after binding to Mo(VI), the amide C=O of the amide–imine conjugate assumes single bond character. Similarly, for **M2**, O004–C00C (1.307(6)Å) and O006–C00G (1.344(7)Å) for amide C–O and phenol C–O are close. The CH=N bond lengths, N006–C00G (1.288(7)Å) and N008–C00H (1.300(7)Å) for **M1** and N007–C00E (1.290(7)Å) and N009–C00C (1.306(7)Å) for **M2** indicate double bond character. Both **M1** and **M2** belong to the triclinic crystal system with space group $P\bar{1}$. two oxo groups, Mo=O, have double bond character in **M1**, *viz.*, Mo–O3 (1.678(5)Å) and Mo–O2 (1.705(5)Å), whereas Mo–O1 (1.695(4)Å) and Mo–O2 (1.693(5)Å) in **M2** are in the *cis*-geometry. Both **M1** and **M2** have a coordination number of six, where water acts as a coordinating solvent in **M1** and methanol in **M2**. The imine nitrogen, N006, two oxygens, O004 and O005 of tridentate **L1**, along with an oxo-group, O2, form the equatorial plane, while the axial positions are fulfilled by O1 from water and O3 of the other oxo-group, defining the distorted octahedron geometry around Mo(VI) in **M1**. The geometry around Mo(VI) in **M2** is also a distorted octahedral, where the equatorial plane is formed by the imine nitrogen, N007, two oxygens, O006 and O004 of tridentate **L2**, along with one oxo-group, O1, whereas the axial positions are occupied by the other oxo-group, O2, and O005 from methanol. Bond angles, O3–Mo1–O4 (170.2(2)°) (**M1**) and O2 Mo01 O005 (170.6(2)°) (**M2**) are 9.8° and 9.4° away from a perfect octahedron.

Spectroscopic studies

The recognition and quantification of calcon and 2-aminobutyric acid using **M1** and **M2** were investigated spectroscopically (emission and absorption) in DMSO/H_2O (4/1, v/v) media.

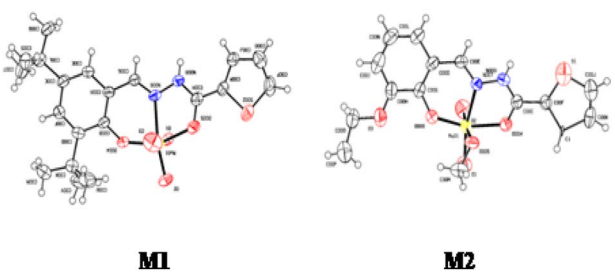

Fig. 1 ORTEP views of M1 and M2.

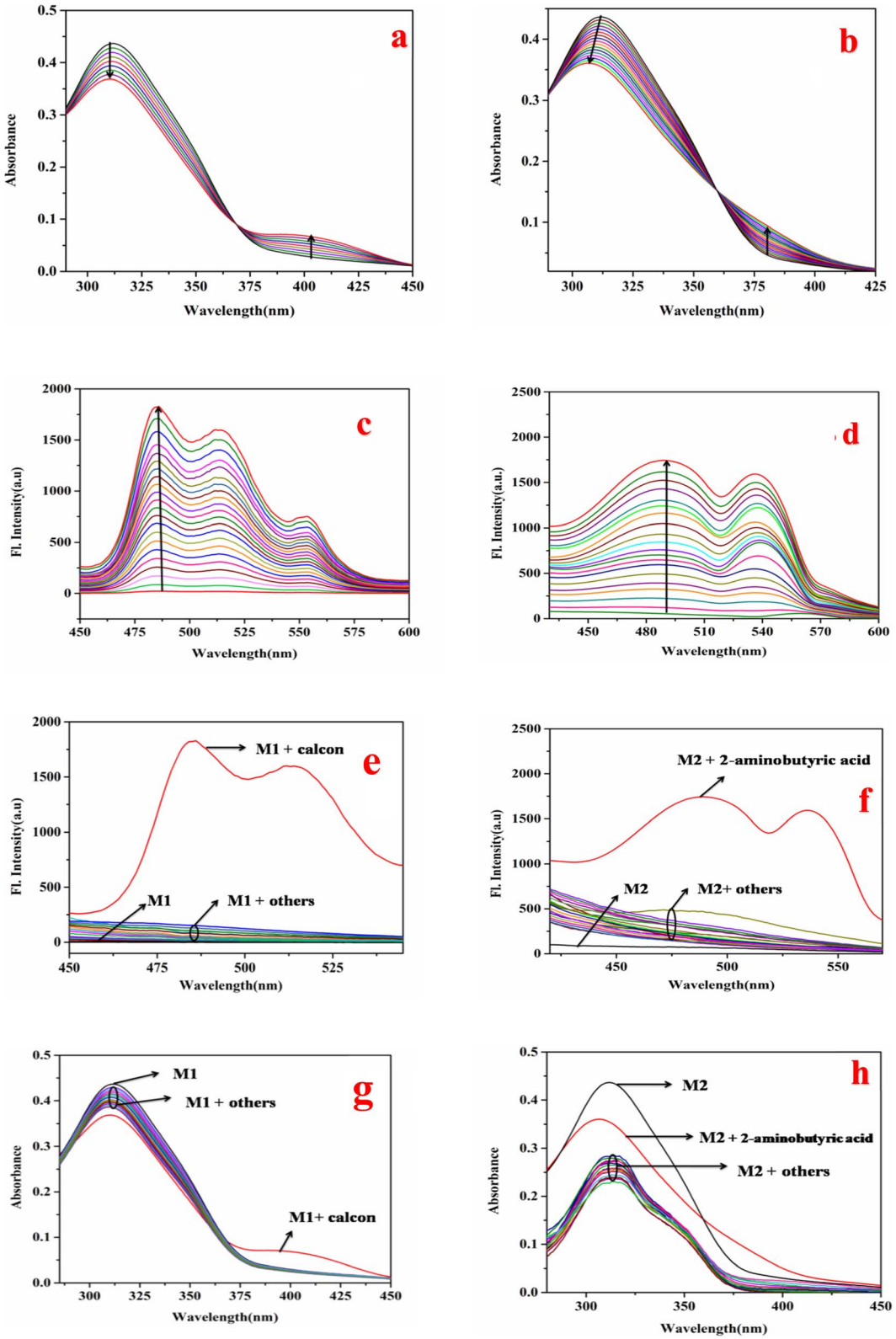

Fig. 2 Spectroscopic studies of **M1** and **M2**. Media: 0.1 M PBS buffer, DMSO/H_2O, 4/1, v/v, and pH 7.4. (a) UV-vis titration plot of **M1** (20 μM) *vs.* calcon (1–2500 μM). (b) UV-vis titration of **M2** (20 μM) *vs.* 2-aminobutyric acid (1–2500 μM). (c) Fluorescence titration plot of **M1** (20 μM, λ_{ex} = 285 nm) *vs.* calcon (1–2500 μM). (d) Fluorescence titration plot of **M2** (20 μM, λ_{ex} = 290 nm) *vs.* 2-aminobutyric acid (1–2500 μM). (e) Effects of common dyes and indicators on the emission spectra of **M1** (20 μM). (f) Effects of natural amino acids and biomolecules on the emission spectra of **M2** (20 μM). (g) Effects of common dyes and indicators on the absorption spectra of **M1** (20 μM). (h) Effects of natural amino acids and biomolecules on the absorption spectra of **M2** (20 μM).

M1 exhibited an absorption peak at 311 nm. Upon gradual addition of calcon (as Na salt) to **M1**, the 311 nm peak decreased significantly with the appearance of a shoulder at 404 nm through an isosbestic point at 368 nm (Fig. 2a).

On the other hand, upon the addition of 2-aminobutyric acid to the solution of **M2** (DMSO/H_2O, 4/1, v/v, PBS buffer, pH 7.4), the absorbance at 312 nm gradually reduced and shifted to 306 nm with the appearance of a new peak at 380 nm along with an isosbestic point at 359 nm (Fig. 2b).

Corresponding emission spectroscopic studies, performed in the mentioned media revealed that the weak emission of **M1** at 484 nm (λ_{ex}, 285 nm) was significantly enhanced upon the addition of calcon (Na salt) (Fig. 2c). Similarly, the weak emission of **M2** at 489 nm (λ_{ex}, 290 nm) was gradually enhanced with increasing 2-aminobutyric acid concentration (Fig. 2d). The enhancement of emission intensity is attributed to the displacement of **L1** and **L2** from **M1** and **M2** by calcon and 2-aminobutyric acid, respectively. The effect of pH on the fluorescence enhancement was tested in the pH range of 2.0 to 12.0 (Fig. S8a and b, SI). The optimum value was observed at ~pH 7.4; hence, all experiments were performed at pH 7.4 (DMSO/H_2O, 4/1, v/v, 0.1 M PBS buffer).

Moreover, it was observed that apart from calcon, other common indicators, *viz.*, murexide, phenolphthalein, EBT, methyl red, methyl orange, thymol blue, bromocresol green, methyl violet, alizarin yellow R, bromothymol blue, anthraquinone, methylene blue, malachite green, picric acid, and rhodamine B, do not affect the emission intensity of **M1** (Fig. 2e).

Apart from 2-aminobutyric acid, other α-amino acids, *viz.*, methionine, arginine, cysteine, proline, lysine, tryptophan, phenylalanine, glycine, alanine, aspartic acid, and biomolecules, *viz.*, creatinine, superoxide dismutase, bisphenol, glutathione, cytochrome C, insulin and uric acid, do not affect the emission spectra of **M2** (Fig. 2f). A similar observation was made during absorption spectroscopic studies (Fig. 2g and h).

The selectivity of **M1** for calcon was tested by measuring the emission intensities of **M1** in the presence of calcon and other indicators in a competitive environment (Fig. S9a, SI).

Likewise, the selectivity of **M2** for 2-aminobutyric acid was tested by monitoring the emission intensity of **M2** in the presence of a mixture of 2-aminobutyric acid with various other amino acids (Fig. S9b, SI). In both cases, no significant effect was observed, indicating the non-interference of competing molecules. Moreover, the same spectra were obtained as for the binary mixtures of **M1**/**M2** with calcon/2-aminobutyric acid, indicating the selectivity of the recognition processes. The plot of emission intensity *vs.* analyte concentration is sigmoidal (Fig. S10a and b, SI). The linear region of the sigmoidal plot is useful in determining the unknown concentration of the analyte at low levels. The limits of detection (LODs) of **M1** and **M2** for calcon and 2-aminobutyric acid were 6 nM and 5 nM, respectively (Fig. S11a and b, SI). The corresponding ligand-displacement constants are 6.2×10^3 M^{-1} and 12.9×10^4 M^{-1}, respectively (Fig. S12a and b, SI). Job plots indicate a 1 : 1 (mole ratio) interaction for both cases (Fig. S13a and b, SI).

A competitive binding experiment was performed to establish the efficiency of ligand displacement in DMSO/H_2O media (4/1, v/v). The binding of calcon with Mo(VI) in the presence of **L1** was monitored by following the emission profile, and the observed binding constant was 9.3×10^3 M^{-1} (Fig. S15a, SI), in close agreement with the displacement binding constant value of calcon with **M1**.

A similar experiment was performed by reacting 2-aminobutyric acid with Mo(VI) in the presence of **L2**, where the binding constant was found to be 15.07×10^4 M^{-1} (Fig. S15b, SI), almost the same as the displacement binding constant value of 2-aminobutyric acid with **M2**. These results firmly establish the proposed ligand-displacement protocol of fluorescence sensing. The release of the fluorescent amide–imine ligand into solution resulted in a significant fluorescence enhancement.

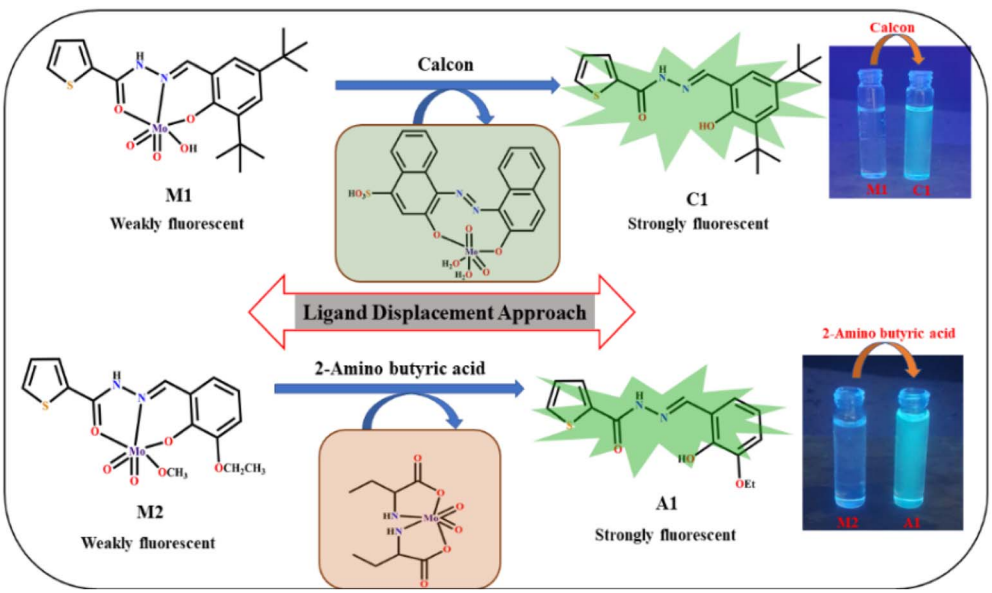

Scheme 2 Plausible sensing mechanism.

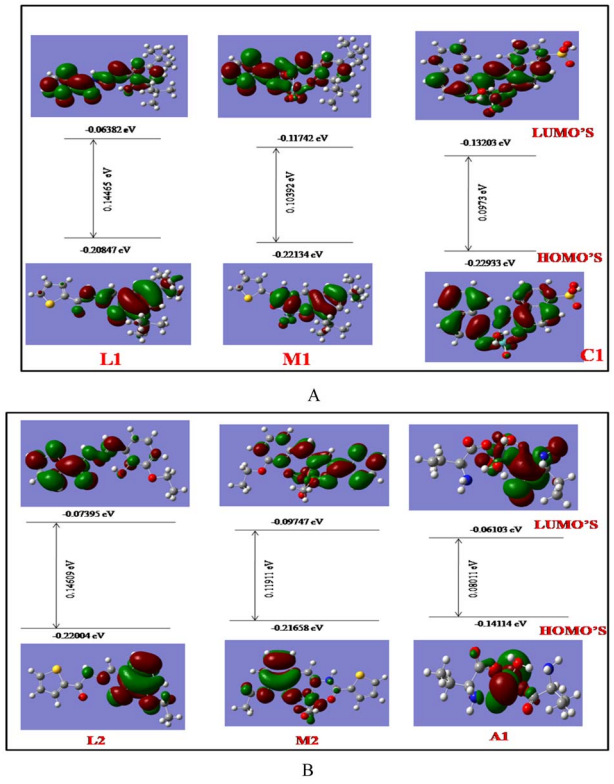

Fig. 3 Frontier molecular orbitals and HOMO–LUMO energy gaps of (A) L1, M1 and C1 and (B) L2, M2 and A1.

Sensing mechanism

Free ligands, **L1** and **L2**, are fluorescent. Upon interaction with Mo(VI) ions, they form the corresponding Mo(VI) complexes, **M1** and **M2**, having very weak fluorescence due to energy transfer and/or electron transfer from the excited state of the fluorescent moiety to the low-lying empty d-orbital of Mo(VI).[45,46] The emission intensities of **M1** and **M2** were enhanced upon the addition of calcon and 2-aminobutyric acid, respectively. This is attributed to the displacement of the fluorescent **L1** and **L2** from **M1** and **M2** by calcon and 2-aminobutyric acid, respectively (Scheme 2).

The emission characteristics involved in the sensing processes have been narrated briefly. **L1**/**L2** (thiophene–amide–imine) is a donor–π–acceptor system where thiophene is the electron donor and amide–imine is the π-acceptor (intramolecular charge transfer, ICT).[47]

When amide–imine derivatives (**L1** and **L2**) coordinate to the Mo(VI) ion through N, O-donors, ICT is perturbed in the resultant coordination complexes, **M1** and **M2**, respectively. Consequently, the fluorescence of **L1** and **L2** was significantly quenched, attributed to the inhibition of ICT and initiation of a PET process from imine-N and/or O-centres to the Mo(VI) (d^0 system). In addition, the heavy Mo(VI) ion enhances intersystem crossing (ISC), favouring non-radiative decay. Overall, both **M1** and **M2** are weakly fluorescent. Upon the addition of analytes, namely, calcon and 2-aminobutyric acid, competitive binding to the Mo(VI) center takes place due to the strong binding affinity of calcon and 2-aminobutyric acid. As a result, displacement of **L1**/**L2** from **M1**/**M2** takes place and consequently, ligand (**L1**/**L2**) → metal (Mo^{VI}) charge transfer processes are inhibited and, ICT processes are restored, leading to the restoration of fluorescence of the **L1**/**L2**. This may be viewed as a PET "off-on" process where complexation enables PET (quenching) and decomplexation inhibits PET (fluorescence restoration).

This proposed mechanism is corroborated by mass and FTIR spectra. The mass spectrum of the system containing **M1** and calcon has peaks at *m*/*z* 574.83 and 366.94, assigned to the [Mo(VI)–calcon] adduct and displaced **L1**, respectively. Similarly, for the system where **M2** and 2-aminobutyric acid are interacting, the peak at *m*/*z* 333.92 is due to the [Mo(VI)-2-aminobutyric acid] species, whereas the peak at *m*/*z* 290.99 is assigned to the displaced **L2**. Job plots also corroborate the ligand-displacement process. The interaction was further rationalized by ^{1}H NMR spectra and DFT studies.

^{1}H NMR spectroscopic studies

The binding interactions between the ligands **L1** and **L2** with Mo(VI) ions resulted in **M1** and **M2**, and further interactions of **M1** and **M2** with calcon and 2-aminobutyric acid were monitored by ^{1}H NMR spectroscopy. It was observed that the phenol –OH (b) peak of **L1** at 12.11 ppm disappeared in **M1** (Fig. S14a, SI). On further interaction of **M1** with calcon, the NMR spectrum changed significantly and resembled that of **L1**, which was displaced from **M1** by calcon.

Identical phenomena were observed during the interaction of **L2** with Mo(VI), leading to **M2** (Fig. S14b, SI), which further interacted with 2-aminobutyric acid. The highly de-shielded phenol –OH (b) at 11.78 ppm of **L2** disappeared upon complexation with Mo(VI), and it reappeared at 10.74 ppm upon displacement by 2-aminobutyric acid from **M2**.

Density functional theoretical (DFT) studies

To unlock the associated orbital energy parameters, DFT studies were performed for the systems, **L1**, **L2**, **M1**, **M2**, **C1** and **A1**, using the TD-SCF/DFT/B3LYP/SDD basis set. The energy gaps between the highest occupied orbital (HOMO) and lowest unoccupied molecular orbital (LUMO) for **L1**, **M1**, and **C1** are shown in Fig. 3A, while those of **L2**, **M2**, and **A1** are presented in Fig. 3B. The HOMO–LUMO energy gap in **L1** is 0.14465 eV, which was reduced to 0.10392 eV in **M1**. Upon interaction with calcon, it further decreased to 0.0973 eV in **C1**.

On the other hand, the HOMO–LUMO energy gap in **L2**, 0.14609 eV, decreased to 0.11911 eV in **M2**, and was further reduced to 0.08011 eV upon interaction with 2-aminobutyric acid, resulting in **A1**. The results clearly indicate a favourable interaction. Important parameters obtained from the DFT studies are presented in Table S3a and b (SI).

Conclusion

Two new Mo(VI) complexes (**M1** and **M2**) have been prepared from two different thiophene-appended amide-based imine derivatives (**L1** and **L2**) and structurally authenticated by single-

crystal X-ray diffraction analysis, in addition to common spectroscopic characterizations. **M1** and **M2** selectively recognize calcon and 2-aminobutyric acid, respectively, *via* 'turn on' fluorescence, following the ligand-displacement protocol. The LODs of **M1** and **M2** for calcon and 2-aminobutyric acid are 6 nM and 5 nM, respectively. DFT studies unlocked the associated orbital energy parameters that support favourable interactions. Thus, this report provides a significant contribution and advancement towards metal complex-based fluorescence recognition of a toxic dye, calcon, and a biomolecule, 2-aminobutyric acid, which may help biomedical researchers.

Author contributions

S. M.: conceptualization, methodology, synthesis of ligands and Mo(VI) complexes, spectroscopic studies, writing – original draft. P. M.: experimental support during spectroscopic measurements and data analysis. A. K. D.: DFT studies. S. C.: formal analysis and visualization. D. D.: supervisor, design idea and planning, MS editing.

Conflicts of interest

There are no conflicts to declare.

Data availability

CCDC 2365489 (**M1**) and 2365810 (**M2**) contain the supplementary crystallographic data for this paper.[48a,b]

All related data are available in the supplementary information (SI), in addition to the text. Supplementary information: ESI-MS, NMR, FTIR, UV-vis, and fluorescence spectra and single crystal X-ray data. See DOI: https://doi.org/10.1039/d6ra02104b.

Acknowledgements

We thank the USIC, BU, for providing access to the SC-XRD facility.

References

1 G. Arthur, *The Amide Linkage: Selected Structural Aspects in Chemistry, Biochemistry, and Materials Science*, Wiley-Interscience, 2000.
2 J. M. Humphrey and A. R. Chamberlin, *Chem. Rev.*, 1997, **97**, 2243–2266.
3 X. Liu, L. Lin and X. Feng, *Chem. Commun.*, 2009, 6145–6158.
4 V. R. Pattabiraman and J. W. Bode, *Nature*, 2011, **480**, 471–479.
5 R. C. Larock, *Comprehensive Organic Transformation*, VCH, New York, 1999, p. 102.
6 S. Roy, S. Roy and G. W. Gribble, *Tetrahedron*, 2012, **68**, 9867–9923.
7 J. Lee, S. K. Muthaiah and S. H. Hong, *Adv. Synth. Catal.*, 2014, **356**, 2653–2660.
8 S. C. Ghosh, J. S. Y. Ngiam, A. M. Seayad, D. T. Tuan, C. L. L. Chai and A. J. Chen, *J. Org. Chem.*, 2012, **77**, 8007–8015.
9 R. Cadoni, A. Porcheddu, G. Giacomelli and D. L. Luca, *Org. Lett.*, 2012, **14**, 5014–5017.
10 D. M. Flanigan, F. Romanov-Michailidis, N. A. White and T. Rovis, *Chem. Rev.*, 2015, **115**, 9307–9387.
11 W. Q. Zhang, A. J. Atkin, I. J. Fairlamb, A. C. Whitwood and J. M. Lynam, *Organometallics*, 2011, **30**, 4643.
12 R. Al-Tohamy, S. S. Ali, F. Li, K. M. Okasha, Y. A. G. Mahmoud, T. Elsamahy, H. Jiao, Y. Fu and J. Sun, *Ecotoxicol. Environ. Saf.*, 2022, **231**, 113160.
13 A. R. Bagheri, M. Ghaedi, A. Asfaram, R. Jannesar and A. Goudarzi, *Ultrason. Sonochem.*, 2017, **35**, 112–123.
14 P. Nuengmatcha, S. Chanthai, R. Mahachai and W. C. Oh, *Dyes Pigm.*, 2016, **134**, 487–497.
15 M. R. Fat'hi and S. J. H. Nasab, *Int. J. Biol. Macromol.*, 2018, **114**, 1151–1160.
16 M. Vinuth, H. S. B. Naik, M. M. M. Swamy, B. M. Vinoda, R. Viswanath and H. Gururaj, *Adv. Mater. Lett.*, 2016, **8**, 49–57.
17 M. Roosta, M. Ghaedi and A. Asfaram, *RSC Adv.*, 2015, **5**(70), 57021–57029.
18 L. A. V. de Luna, T. H. G. da Silva, R. F. P. Nogueirab, F. Kummrow and G. A. Umbuzeiro, *J. Hazard Mater.*, 2014, **276**, 332–338.
19 M. Punzi, F. Nilsson, A. Anbalagan, B. M. Svensson, K. Jönsson, B. Mattiasson and M. Jonstrup, *J. Hazard. Mater.*, 2015, **292**, 52–60.
20 M. Zarei-Chaleshtori, V. Correa, N. López, M. Ramos, R. Edalatpour, N. Rondeau and R. R. Chianelli, *J. Catal.*, 2014, **4**, 346–355.
21 A. Asfaram, M. Ghaedi, M. H. Ahmadi Azqhandi, A. Goudarzi and Sh. Hajati, *J. Ind. Eng. Chem.*, 2017, **54**, 377–388.
22 C. I. Pearce, J. R. Lloyd and J. T. Guthrie, *Dyes Pigm.*, 2003, **58**, 179–196.
23 J. W. Lee, S. P. Choi, R. Thiruvenkatachari, W. G. Shim and H. Moon, *Dyes Pigm.*, 2006, **69**, 196–203.
24 S. Saha and A. Pal, *Sep. Purif. Technol.*, 2014, **134**, 26–36.
25 M. Jafari, M. R. Rahimi, M. Ghaedi, H. R. Javadian and A. Asfaram, *J. Colloid Interface Sci.*, 2017, **507**, 172–189.
26 R. Mallampati, L. Xuanjun, A. Adin and S. Valiyaveettil, *ACS Sustain. Chem. Eng.*, 2015, **3**, 1117–1124.
27 R. Giovannetti, E. Rommozzi, C. A. D'Amato and M. Zannotti, *J. Catal.*, 2016, **6**, 84.
28 X. Liu, Q. Zhang, B. Yu, R. Wu, J. Mai, R. Wang, L. Chen and S.-J. Yang, *J. Catal.*, 2016, **6**, 146.
29 Q. Ge, P. Wang, C. Wan and T. S. Chung, *Environ. Sci. Technol.*, 2012, **4**, 6236–6243.
30 A. Asfaram, M. Ghaedi, G. R. Ghezelbash and F. Pepe, *Ecotoxicol. Environ. Saf.*, 2017, **139**, 219–227.
31 I. Ali, *Chem. Rev.*, 2012, **112**, 5073–5091.
32 Y. Kan, Q. Yue, J. Kong, B. Gao and Q. Li, *Chem. Eng. J.*, 2015, **260**, 541–549.
33 S. Mazaheri, S. M. Ghoreishi and M. Motaghedifard, *J. Mol. Liq.*, 2016, **219**, 883–889.

34 S. Das, S. Guha, A. Banerjee, S. Lohar, A. Sahana and D. Das, *Org. Biomol. Chem.*, 2011, **9**, 7097–7104.
35 J. Das, S. Ta, N. Salam, S. Das, S. Ghosh and D. Das, *RSC Adv.*, 2023, **13**, 13195.
36 S. Khanra, S. Ta, A. Paladhi, M. Ghosh, S. Ghosh, S. K. Hira, P. P. Manna, P. Brandão, V. Félix and D. Das, *Chem. Commun.*, 2020, **56**, 6563–6566.
37 D. L. Ma, V. P. Y. Ma, D. S. H. Chan, K. H. Leung, H. Z. He and C. H. Leung, *Coord. Chem. Rev.*, 2012, **256**, 3087–3113.
38 H. Matsui and H. Ohtaki, *Bull. Chem. Soc. Jpn.*, 1982, **55**, 461–465.
39 C. Djordjrvic, N. Vulteic, B. A. Jacobs, M. Lee-Renslo and E. Sinn, *Inorg. Chem.*, 1997, **36**, 1798–1805.
40 S. Ta, M. Ghosh, N. Salam, J. Das, M. Islam, P. Brandão, V. Félix, J. Sanmartin and D. Das, *Appl. Organomet. Chem.*, 2020, e5823.
41 M. C. Burla, R. Caliandro, M. Camalli, B. Carrozzini, G. L. Cascarano, L. De Caro, C. Giacovazzo, G. Polidori and R. Spagna, *J. Appl. Crystallogr.*, 2005, **38**, 381–388.
42 G. M. Sheldrick, *Acta Crystallogr.*, 2008, **E64**, 112–122.
43 G. M. Sheldrick, *Acta Crystallogr.*, 2015, **A71**, 3–8.
44 O. V. Dolomanov, L. J. Bourhis, R. J. Gildea, J. A. K. Howard and H. Puschmann, *J. Appl. Crystallogr.*, 2009, **42**, 339–341.
45 O. Sahin and M. Yilmaz, *Tetrahedron*, 2011, **67**, 3501–3508.
46 L. J. Tang and M. J. Cai, *Sens. Actuators, B*, 2012, **173**, 862–867.
47 I. A. Rather and R. Ali, *Org. Biomol. Chem.*, 2021, **19**, 5926.
48 (*a*) CCDC 2365489: Experimental Crystal Structure Determination, 2026, DOI: 10.5517/ccdc.csd.cc2kdh3l; (*b*) CCDC 2365810: Experimental Crystal Structure Determination, 2026, DOI: 10.5517/ccdc.csd.cc2kdtg8.